Design of a Laboratory Hall Thruster with Magnetically Shielded Channel Walls, Phase I: Numerical Simulations

Ioannis G. Mikellides,* Ira Katz,† Richard R. Hofer‡
Jet Propulsion Laboratory, California Institute of Technology, Pasadena, CA, 91109

Abstract: In a proof-of-principle effort to demonstrate the feasibility of magnetically shielded (MS) Hall thrusters, an existing laboratory thruster has been modified with the guidance of physics-based numerical simulation. When operated at a discharge power of 6-kW the modified thruster has been designed to reduce the total energy and flux of ions to the channel insulators by >1 and >3 orders of magnitude, respectively. The erosion rates in this MS thruster configuration are predicted to be at least 2-4 orders of magnitude lower than those in the baseline (BL) configuration. At such rates no detectable erosion is expected to occur.

I. Introduction

Hall thrusters provide an attractive combination of thrust and specific impulse for a variety of near-earth missions and, in many cases, they allow for significant reductions in propellant mass and overall system cost compared to chemical propulsion. Hall thrusters also could enable a variety of deep-space science missions of interest to NASA due to the range of thrust and specific impulse they are capable of attaining. Yet, these thrusters have never flown onboard NASA spacecraft largely because deep-space missions require, in general, wider throttling and higher propellant throughput. A critical wear processes known to exist in Hall thrusters that has limited their applicability to near-earth applications is erosion of the acceleration channel.

Channel erosion had been recognized as a potential limitation of Hall thrusters for space missions early in their history. Although propulsive performance dominated their development early on, techniques to reduce or eliminate erosion were considered as early as the 1960s. In an extensive review of stationary plasma thrusters (SPT) published in 2000, Morozov and Savelyev state: "*…at the beginning of the 1960s magnetic-force-line equipotentialization became known, and the chosen geometry of force lines (convex toward the anode) provided repulsion of ions from the walls by the electric field, thus reducing the channel erosion*."[1] Indeed, the advanced magnetic field topologies that are being used in many state-of-the-art (SOA) Hall thrusters today have led to improvements both in performance and wear.[2,3,4,5,6] However, channel erosion has not been eliminated or reduced sufficiently to retire the risk for deep-space science missions.

In most conventional Hall thrusters the acceleration channel (also known as the discharge chamber) is formed by the anode and two (inner and outer) rings made of electrically insulating material. Recently, during a Qualification Life Test[7] (QLT) of a commercial Hall thruster called the BPT-4000 it was observed that the erosion of the channel insulators practically stopped, reaching a near-steady state after ~5,600 h. The reasons the channel stopped eroding were unclear. Soon thereafter, numerical simulations performed with a two-dimensional (2-D) axisymmetric plasma solver[8] revealed that when the channel receded from its early-in-life to its steady-state configuration the following changes occurred near the walls: (1) reduction of the electric field parallel to the wall that prohibited ions from acquiring significant impact kinetic energy before entering the sheath, (2) reduction of the potential fall in the sheath that further diminished the total energy ions gained before striking the material and, (3) reduction of the ion number density that decreased the flux of ions to the wall.[9] All these changes were found to have been induced by the magnetic field and constituted, collectively, an effective shielding of the walls from any significant ion bombardment. It was proposed then that "magnetically shielded" (MS) channel insulators could be designed as part of a new generation of Hall thrusters capable of having many times to orders of magnitude the life capability of their SOA counterparts. Mikellides *et al*.9 also argued that such "magnetic shielding" is distinctively different from other

* Member of the Technical Staff, Electric Propulsion Group, 4800 Oak Grove Drive, Pasadena, CA, 91109, Mail Stop 125-109, Associate Fellow AIAA.
† Group Supervisor, Electric Propulsion Group, 4800 Oak Grove Drive, Pasadena, CA, 91109, Mail Stop 125-109, Senior Member AIAA.
‡ Member of the Technical Staff, Electric Propulsion Group, 4800 Oak Grove Drive, Pasadena, CA, 91109, Mail Stop 125-109, Senior Member AIAA.

techniques currently being pursued to protect surfaces from erosion, like in the Highly Efficient Multistage Plasma Thruster (HEMP-T)[10] and the Diverging Cusped Field Thruster (DCFT).[11] These configurations exploit the magnetic mirror effect on electrons by employing multi-cusped magnetic fields to reduce plasma bombardment of the walls at the cusps. Such cusped arrangements provide also the magnetic field direction needed to induce the azimuthal electron motion and, in turn, the accelerating electric field at the cusped regions. In Hall thrusters with MS channel walls there is no magnetic mirror effect because there are no cusps.

Magnetic shielding takes advantage of the equipotentialization of the magnetic field lines and applies them in a way that sustains high plasma potential near the channel surfaces, in fact, as close as possible to the discharge voltage. In this manner the kinetic energy that ions gain through the potential fall along surfaces can be reduced significantly. Moreover, with a properly designed combination of field topology and channel geometry the electric field vectors can be made both nearly perpendicular to the surface and very large in magnitude to force significant ion acceleration away from walls without loss of propulsive performance. This can reduce the wall-incident ion flux by several orders of magnitude.9 The fundamental principle behind magnetic shielding lies in the recognition that "equipotentialization" implies it is the sum of two quantities that remains constant along magnetic field lines: the plasma potential and the contribution from the electron pressure, $T_e \times \ln(n_e)$; Morozov1 termed the sum of these two quantities "thermalized potential." To remain consistent with this original terminology we shall refer to the related property of the magnetic field lines hereinafter as "thermalized equipotentialization." If significant, the contribution of the electron pressure will produce deviations from orthogonality between the electric and magnetic fields such that the "…*geometry of force lines (convex toward the anode)*…"1 can no longer act effectively to control the electric field near surfaces and, in turn, the erosion. In essence magnetic shielding eliminates the contribution of the electron pressure by exploiting those magnetic field lines that extend deep into the acceleration channel. These lines are therefore associated with high plasma potential and low electron temperature, a combination that marginalizes the contribution of $T_e \times \ln(n_e)$.

The QLT *ex post facto* numerical simulations revealed a technique by which the life of Hall thrusters could be extended significantly, and in 2009 a proof-of-principle effort began at the Jet Propulsion Laboratory (JPL) to demonstrate its feasibility. Development of a new thruster was beyond the scope of this effort. Therefore, our approach was to modify the channel geometry and magnetic field of an existing thruster - a 6-kW laboratory Hall thruster called "H6" - with the guidance of physics-based numerical simulation. Hereinafter we shall term this modified version of the thruster the "MS configuration." Numerical simulations and thruster modifications have constituted phase I of the design effort. In the (ongoing) phase II we plan to determine erosion rates from direct measurements along the channel insulators in both configurations, at a single operating condition. This paper focuses on the first phase of the effort. The numerical simulations of the partially ionized gas in the two configurations have been performed with the Hal2De code,8 a 2-D axisymmetric solver developed at JPL that uses a magnetic-field-aligned computational mesh (MFAM). Sections II-A and II-B provide a brief description of Hall2De and recent code augmentations. Sections II-C and II-D discuss plasma simulation results. Whenever possible, comparisons with past measurements are reported in these sections also. Section II-E compares computed erosion rates along the acceleration channel insulators. We conclude in Sec. III with a description of the thruster tests and diagnostics planned for the second and final phase of the effort.

II. Design of a Magnetically Shielded Hall Thruster Using Physics-based Numerical Simulation

A. General description of the Hall2De code

Hall2De is a 2-D computational solver of the conservations equations that govern the evolution of the partially ionized gas in Hall thrusters. The code is a descendant of OrCa2D, a 2-D computational model of electric propulsion hollow cathodes that employs a combination of implicit and explicit algorithms to solve numerically the conservation laws in these devices.[12,13] The governing equations, numerical methodology, simulation results and comparisons with performance and plasma measurements have been presented elsewhere.8,9 Here, we provide a brief overview of the code and report on recent advances in the physics and numerics of the code.

In Hall2De excessive numerical diffusion due to the large disparity of the transport coefficients parallel and perpendicular to the magnetic field is evaded by discretizing the equations on a computational mesh that is aligned with the applied magnetic field. This MFAM capability was largely motivated by the need to assess the life of Hall thrusters with complicated magnetic field topologies. The MFAM and ionized gas solvers comprise Hall2De. The main components, input/output (I/O) and high-level flowchart of the solver are depicted in Figure 1.

Although there are many similarities between Hall2De and other solvers like the well-known Hybrid-Particle-in-Cell Hall ("HPHall")[14,15] code, there are also several distinctive features in both the physics and the numerical

approach. Such features have been incorporated in Hall2De after many lessons learned from Hall thruster simulations over the last decade. Due to the long history and wide use of HPHall we find it most instructive to outline the major distinctive features of Hall2De compared to HPHall; there are three:

(1) discretization of all conservation laws on a MFAM,
(2) numerical solution of the heavy-species conservation equations without invoking discrete-particle methods
   a) multiple ion fluids can be included each being treated as an isothermal, cold (relative to the electrons) fluid accounting for the drag force and ion pressure gradient,
   b) the evolution of the (collisionless) neutral species is computed using line-of-sight formulations that account for ionization,
(3) large computational domain that extends several times the thruster channel length in the axial direction and encompasses the cathode boundary and the axis of symmetry.

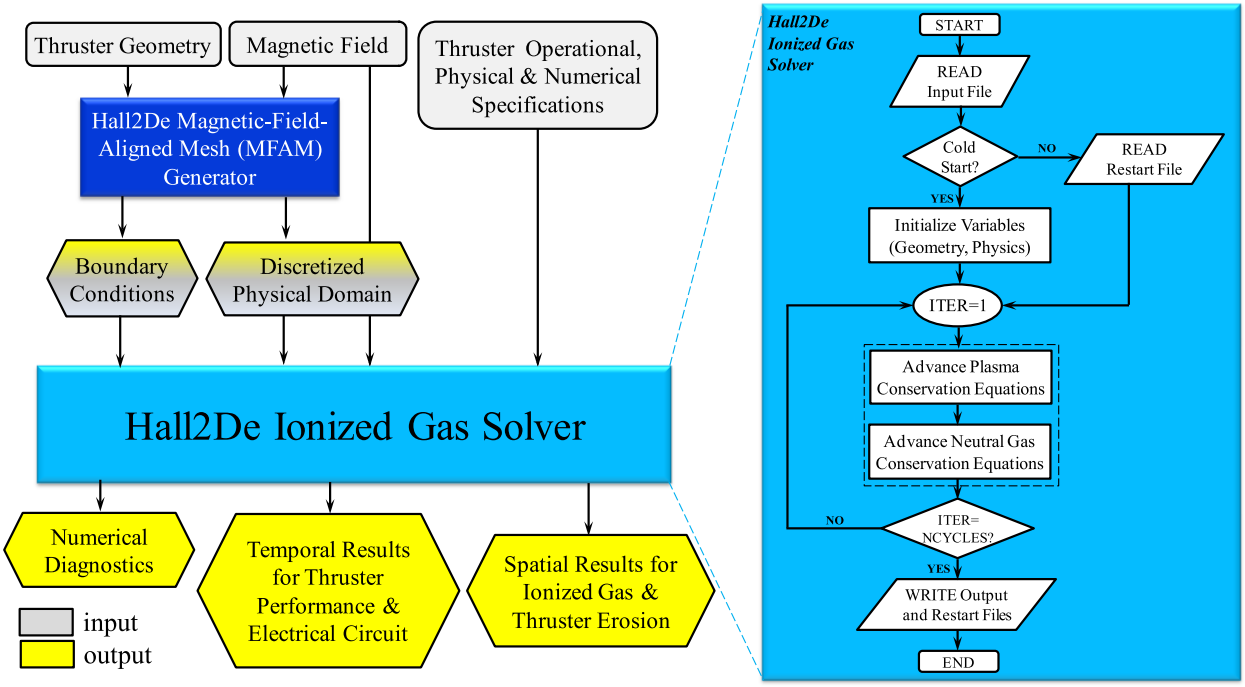

Figure 1. Main components of the Hall2De code, I/O and high-level flowchart of the ionized gas solver.

The first feature allows for the assessment of erosion in regions with complex magnetic field topologies. In regions of the thruster where isothermalization and thermalized equipotentialization of the lines of force persists, the main distinction between Hall2De and HPHall regarding computational approach is that in HPHall a computational element is defined by two lines of force and two boundary segments (and the solution is then interpolated onto an arbitrary structured mesh), whereas in Hall2De such computational element would be further divided into additional elements using an orthogonal set of lines. The equations are then solved on each one of these additional elements. The main advantage here is the ability to simulate regions of the thruster where surfaces have disrupted the lines of force. The MFAM also allows for the self-consistent simulation of the plasma in the near-anode region; unlike HPHall, no magnetic field streamline in this region of Hall2De need be identified upstream of which the conservation laws for the plasma are not solved self-consistently.

The second feature eliminates the inherent statistical fluctuations typically caused by particle-based methods, and the third allows for the investigation of the large-scale behavior of electrons in the plume while accounting for the cathode boundary conditions self-consistently. Shown in Figure 2-left is a schematic of the computational domain for the H6 simulations with naming conventions of various thruster components and boundaries to be cited in this paper. Also, because the main objective in the new design is to protect the magnetic circuit components from plasma bombardment, Figure 2-left and all other 2-D plots in this paper point out (for reference) the locations of the magnet corners relative to the channel insulators. Figure 2-right shows a photograph of the thruster operating in a vacuum facility at JPL.

B. **Physics, numerical approach and recent augmentations in Hall2De**

The evolution of ions in Hall2De is computed using a hydrodynamic approach that accounts for up to triply-charged ions and up to four distinct ion fluids. The latter implies that more than one ion momentum equations can be solved in Hall2De. This multi-fluid capability was developed in recognition of the disparate equilibration times that ions may possess, especially in the near-plume and cathode regions of the thruster. Such disparity can lead to ion populations with displaced Maxwellian distribution functions relative to each other in which case multiple ion conservation equations must be solved. In the present study only a single ion fluid has been considered. The momentum equation is expressed in non-conservative form and fluxes at the four faces of each computational element are estimated using a first-order upwind scheme. Both the ion pressure gradient force and the drag force on ions due to collisions with other heavy species are included. The momentum and continuity equations are marched forward in time explicitly. The velocities are defined at the vertices of each quadrilateral computational element. The code has been upgraded to include contributions from Coulomb collisions of ions of different charge states and of different fluids. The ion conservation laws are closed with conditions specified at all boundaries in Figure 2-left as described in Refs. 8 and 9.

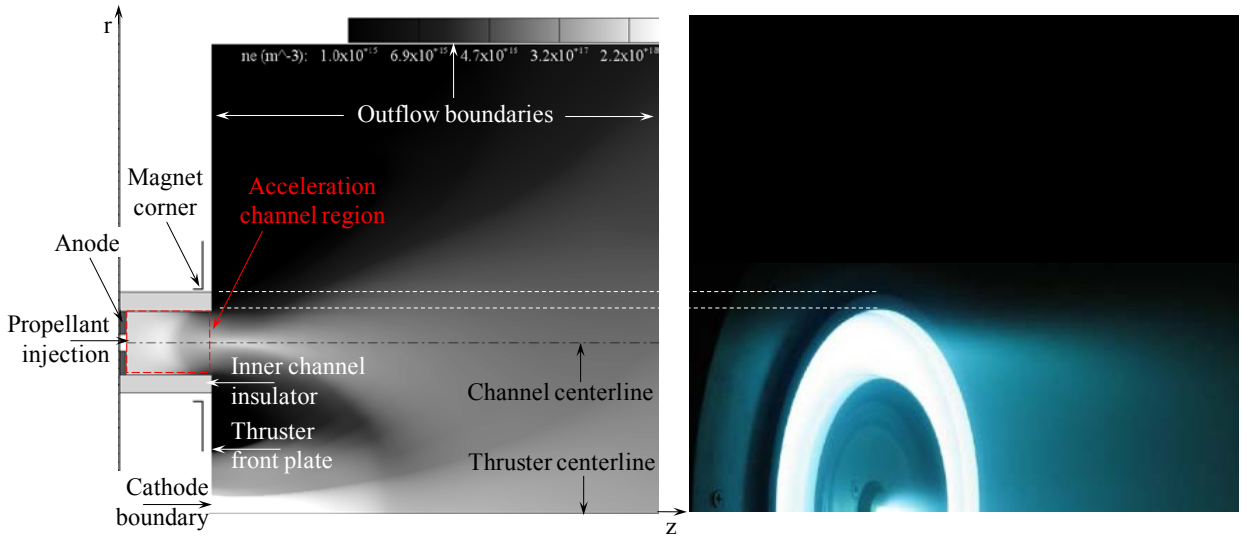

Figure 2. Left: Computational domain for the numerical simulations of the H6 laboratory Hall thruster showing naming conventions for various thruster components and boundaries to be cited throughout this paper. Right: Photograph of the thruster operating in a vacuum facility at JPL.

The electron population in Hall2De is treated also as a fluid. The vector form of Ohm's law is solved in the frame of reference of the magnetic field and the electrical resistivity accounts for contributions from collisions of electrons with all other species. It has also been suggested that the diffusion of electrons in Hall thrusters is enhanced in a non-classical manner by plasma turbulence (e.g. see Refs. 14, 16, 17, 18). Attempts to emulate this enhancement in numerical simulations with HPHall and similar codes have been made typically through the use of an effective collision frequency, which we term here "ν_α". Fife and Martínez-Sánchez proposed[14] that ν_α in Hall thrusters may be based on Bohm's 1/B scaling for the cross-field mobility.[19] In early numerical simulations of SPTs it was typical to use a coefficient to adjust the value of ν_α while retaining its proportionality with the electron cyclotron frequency ω_{ce}. In this work we have imposed the general function $f_\alpha(r,z)$ to define $\nu_\alpha \equiv f_\alpha \omega_{ce}$. In previous simulations with Hall2De in which the profile of ν_α was determined by plasma data, we found large deviations of f_α from a constant value in the near-plume region and therefore little to no correlation of ν_α with ω_{ce} in this region. We have found similar deviations in our present simulations. Finally, to account for wall collisions another effective collision frequency, ν_{ew}, is included that is dependent upon the electron secondary yield. The model is described in greater detail in Ref. 9.

The electron energy conservation equation in Hall2De accounts for thermal conduction, energy exchange between electrons and the heavy species due to deviations from thermal equilibrium,[20] inelastic energy losses due to ionization and excitation.[21] The conservation equations for the electrons are closed with boundary conditions (BC) at all surfaces in Figure 2-left. The channel ring walls and the thruster front plate are dielectric boundaries. At the

anode the previous Dirichlet BCs have been changed to sheath BCs for the electron current density normal to the anode: $j_e=-j_{Te}\exp[-e(\phi-V_A)/k_BT_e]$ for $\phi>V_A$ (electron repelling sheath) where $j_{Te}=en_e(8k_BT_e/\pi m_e)^{1/2}/4$ is the electron thermal current density and k_B is Boltzmann's constant. The electron charge, plasma potential, anode voltage and electron temperature are denoted by e, ϕ, V_A, and T_e, respectively. The new formulation is employed in an implicit fashion in the potential solver. We have found that the major distinction between the two BCs (Dirichlet versus sheath) is higher plasma potential near the anode when sheath BCs are employed, which is to be expected since the electron thermal current density integrated over the anode area is much higher than the discharge current in these devices. At the cathode boundary the neutral particle flux, ion flux, plasma potential and electron temperature are specified directly. For all dielectric-wall boundaries a zero-current condition is imposed. At these surfaces the convective heat loss BC follows the formulations of Hobbs and Wesson[22] for the potential drop in the sheath with secondary electron emission. The energy equation is solved in a semi-implicit fashion; the thermal conduction term is implicit whereas all other terms are evaluated explicitly.

In Hall thrusters the neutral species are collisionless. In Hall2De their evolution is computed with an algorithm that eliminates discrete-particle statistical fluctuations.[23] The algorithm takes advantage of the fact that the majority of neutral particles proceed along straight-line, constant-velocity trajectories until they are either ionized, strike a wall, or leave the physical domain. The algorithm assumes that the particle velocity distribution function for neutrals emitted from a given surface remains unchanged except for a scale factor that reflects the loss of neutrals by ionization. Then the algorithm solves for the neutral gas density by integrating forward in time the linear Boltzmann equation in the absence of any forces on the particles. The sources of neutrals are gas inlets and isotropic, thermally-accommodated propellant atoms emanating from thruster surfaces. Emission from solid boundaries accounts for ions that recombined with electrons at the surface.

In addition to its key role in theoretical investigations of fundamental Hall thruster physics, Hall2De has been developed to guide the design of Hall thrusters and to support their qualification for space flight. These objectives have motivated an upgrade of Hall2De with two new computational capabilities in an effort to reduce time and cost in the design and qualification of these thrusters. The first capability is a fast MFAM generator that allows interactive mesh generation through the use of a graphics user interface (GUI). Specification of the boundary conditions also is performed with this tool. The inputs to the mesh generator are the geometry of the computational region and a magnetic field map in the r-z plane (see also Figure 1). The latter is used to define mesh lines parallel and perpendicular to the magnetic field, which may be added/deleted interactively providing the user full control over the resolution of the grid. This is a valuable design capability because in most cases the strongly shielded regions in MS Hall thrusters will encompass complex magnetic field topologies with highly curved and highly concentrated lines. Naturally then, it will often require several iterations before these regions are discretized adequately. A typical set of magnetic field streamlines in the H6 thruster are plotted in Figure 3-left. The corresponding computational mesh produced by the new MFAM generator is shown in Figure 3-right.

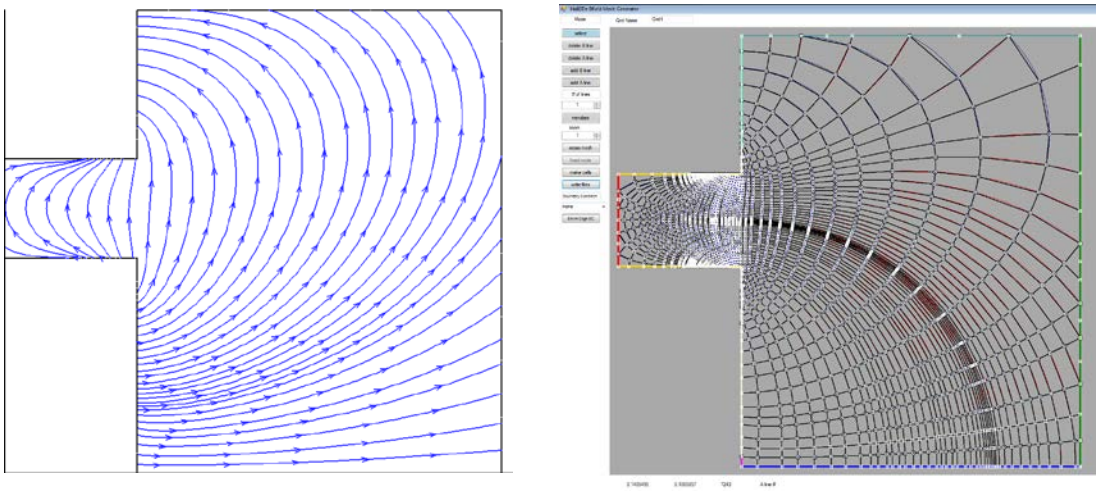

Figure 3. A new magnetic field mesh generator has been developed for Hall2De to facilitate rapid thruster design. Each mesh streamline is generated individually providing the user full control over the discretization of the physical domain. Boundary conditions also are specified in the mesh generator. Left: typical set of magnetic field streamlines in the H6 Hall thruster. Right: MFAM generator window showing corresponding field-aligned computational mesh. Colored boundaries indicate different boundary conditions.

The second new capability allows for execution of a simulation from arbitrary initial conditions ("cold starts"). Presently, a uniform neutral gas at ambient density is specified throughout the computational domain before execution. Then injection of propellant is allowed through the anode boundary and the conservation laws for the neutral gas are marched forward in time until the solution reaches a steady state. In the absence of the plasma the completion of this stage requires relatively small computation time (~several minutes) because a much larger time step may be taken compared to that imposed by the Courant condition for ions. Then, a uniform ("seed") electron number density is specified in the entire computational domain. Concurrently, generic axial profiles are prescribed along the channel centerline for the electron temperature and plasma potential that allow for the specification of these variables in 2-D space. During this initialization phase, magnetic field lines are assumed to be isothermal and equipotential (we note in the absence of a non-uniform electron number density the lines of force are indeed also lines of equal potential). This completes the second stage of the domain initialization at which time (t=0) the full set of conservation laws for the partially ionized gas is marched forward in time. The evolution of the electron number density in the H6 BL configuration is shown in Figure 4. The addition of the new MFAM generator and cold-start capabilities have reduced the time associated with the design iteration cycle by about one order of magnitude.

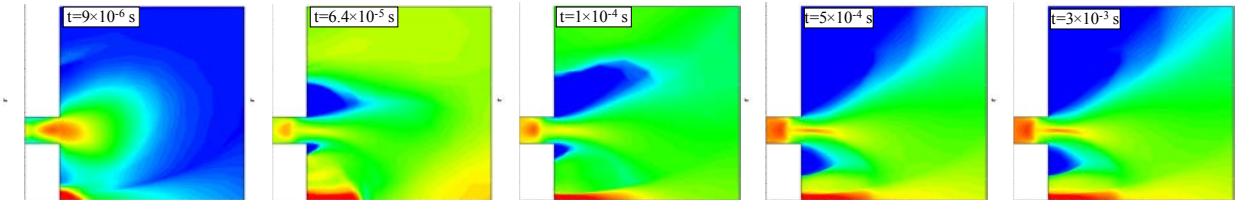

Figure 4. Evolution of the Hall2De solution from a "cold start." Plotted are 2-D contours of the electron number density at different simulation times.

C. Numerical simulations of the baseline thruster

In this section we present numerical simulations of the H6 thruster in its BL configuration at discharge voltage (V_d) of 300 V and discharge current (I_d) of 20 A (Table 1). The BL design has a relatively simple channel geometry (compared to other thrusters like the BPT-4000[5-7]) and the hollow cathode is located at the thruster centerline as shown in Figure 2. This cathode-thruster arrangement is of great interest in numerical simulations because it is 2-D axisymmetric and therefore plasma measurements[24,25] can be compared directly with the simulation results. The operational characteristics of the BL configuration, measured performance, and comparisons with the Hall2De results are provided in Table 1. The ion currents for the three charge states are denoted by I_i^+, I_i^{2+} and I_i^{3+}, and the ion beam flow rate is $\dot{m}_b$. Additional information about the thruster is provided in Sec. III. The maximum axial and radial dimensions of the computational domain are $(z/L)_{max}$=6.25 and $(r/L)_{max}$=5.5, respectively where L denotes the length of the acceleration channel region (see Figure 2). The 2-D simulation results for the electron number density and temperature are shown in Figure 5. Representative magnetic field lines are also shown in Figure 5–right to illustrate the isothermalization of lines in the acceleration channel and the near-plume regions of the thruster.

Table 1. Comparisons of computed and measured[26] performance parameters in the H6 Hall thruster at discharge power of 6 kW. Laboratory experiments with the MS thruster design are ongoing.

Thruster Design	BL		MS
Experiment vs. Theory	Experiment	Theory	Theory
Anode flow rate, $\dot{m}_A$ (mg/s)	19.2	19.2	19.2
Cathode flow rate (mg/s)	1.34	1.34	1.34
Discharge voltage, V_d (V)	300	300	300
Discharge current, I_d (A)	20	20	20
Thrust (mN)	396	376	357
Beam current, I_b (A)	16.3	16.9	16.2
Xe^+ current fraction, I_i^+/I_b	0.75	0.640	0.602
Xe^{2+} current fraction, I_i^{2+}/I_b	0.18	0.318	0.344
Xe^{3+} current fraction, I_i^{3+}/I_b	0.07	0.042	0.054
Mass utilization, $\dot{m}_b/\dot{m}_A$	0.913	0.985	0.913
Current utilization, I_b/I_d	0.815	0.850	0.810

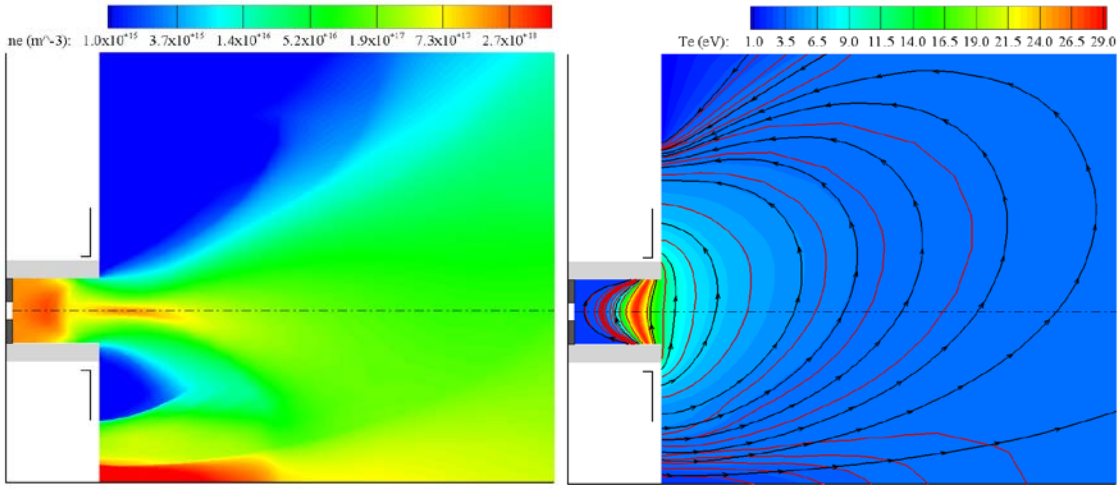

Figure 5. 2-D contours of the electron number density (left) and electron temperature (right) in the BL thruster configuration. The contoured plot for the electron temperature is overlaid by magnetic field streamlines to illustrate their isothermal properties in regions of the thruster where $\Omega_e>>1$. Selected T_e-contours are illustrated in solid red lines. To allow for the self-consistent determination of the electron temperature in regions (like the cathode near-plume) where deviations from isothermality may occur, Hall2De does not specify *a priori* that the electron temperature remains fixed along magnetic field lines.

The comparison of measured and computed profiles for the electron temperature and plasma potential along the channel centerline is shown in Figure 6-left. Since the physics of electron transport from the cathode to the acceleration channel remain unclear today, despite decades of research on this topic, the Hall2De plasma solution is in part dependent upon the collision frequency ν_α the profile of which is plotted in Figure 6-right. By contrast to our previous simulations of the BPT-4000,9 the profiles used in the H6 series of simulations have (1) employed along the channel centerline a continuous function f_α of the form $\exp(-|\underline{z}|^\alpha/\beta)$ with $\underline{z}\equiv(z-z_0)/L$, to eliminate unphysical discontinuities in the first derivatives of the plasma properties and, (2) the electron Hall parameter $\Omega_e=e|B|/m_e\nu_e$ in the thruster plume was computed self-consistently without altering its dependence on ν_e. Here, ν_e denotes the total electron collision frequency as defined in Ref. 9 and m_e is the electron mass. As in many other Hall thruster simulations (e.g. see Refs. 27,28), ν_α in Hall2De has been based on plasma measurements. Specifically, the constants z_0, α and β that determine the spatial variation of f_α have been guided by the electron temperature and plasma potential measurements[25] (Figure 6-left). Then, iteration until the operating discharge current was attained determined the peak value of f_α.

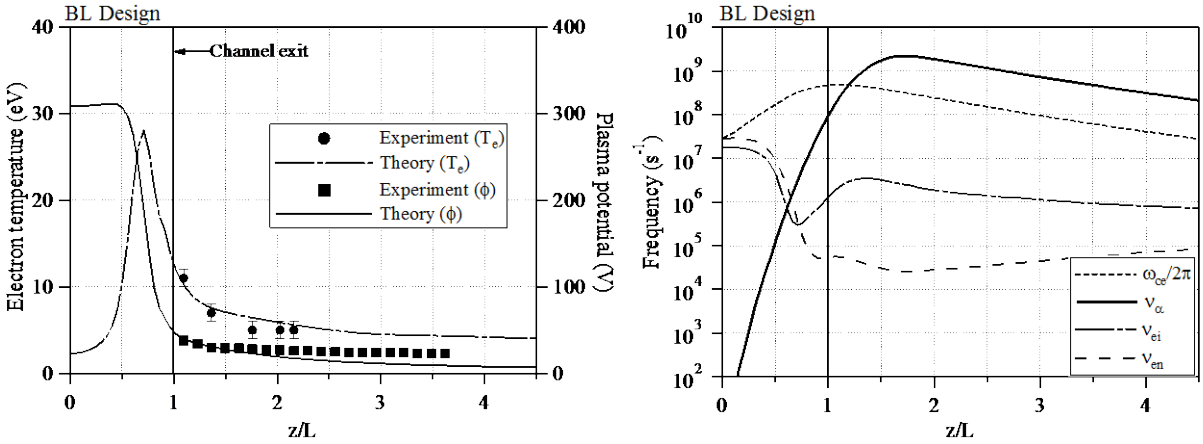

Figure 6. Axial profiles along the channel centerline in the BL configuration of the H6 Hall thruster. Left: Comparisons between numerical simulation results and measurements for the electron temperature and plasma potential. Right: Computed electron-ion (ν_{ei}) electron-neutral (ν_{en}) and non-classical (ν_α) collision frequencies. Also plotted for reference is the electron cyclotron frequency $\omega_{ce}/2\pi$.

Regarding thruster performance and related integrated parameters the BL simulation results for the thrust and beam current are within ~5% of the measured values (see Table 1). The most noticeable discrepancies are associated with the thruster currents as was the case with the BPT-4000 simulations.9 Specifically, we find a consistent over prediction of the doubly-charged ion current fraction and an under prediction of the singly-charged fraction. The accuracy of integrated quantities involving the ion velocity and flux is presently reduced in Hall2De due to the first-order-accurate scheme of the spatial derivatives in the ion momentum equations. It is well-known that first-order upwind discretization is acceptable for flows that are closely aligned with the mesh (e.g. purely axial or purely radial flow in a 2-D rectilinear mesh with quadrilateral elements) but that accuracy decreases due to numerical diffusion as the angle between streamlines and mesh lines increases. In the Hall thruster the angle between the ion-flow streamlines and the normal to the magnetic field lines increases in general with distance from the channel exit. Implementation of a second-order-accurate scheme for the spatial convective derivatives of the ion momentum equations is planned in the near future.

D. **Magnetically shielded thruster**

The first principles of magnetic shielding in Hall thrusters have been described in detail elsewhere.9 In summary, the technique exploits the thermalized equipotentialization and isothermalization of the magnetic field lines in these devices to sustain high plasma potential and low electron temperature along the channel surfaces. The effectiveness of the shielding depends in general on the magnitude of the magnetic field and its local topology relative to the channel geometry. We note that although shielding *can* be achieved if the magnetic field lines are parallel to the wall, such arrangement is not necessary. In the freehand drawings below we show schematically several configurations to clarify our point. For example, in Figure 7-middle the lines are nowhere close to being parallel to any of the surfaces yet this configuration could provide significant shielding of the surfaces from erosion. In the schematic on the right the lines are near parallel to the diverging section of the wall and this configuration too could provide significant shielding of the diverging wall section. By contrast, the field topology relative to the walls at the channel exit in the left and right configurations of Figure 8 does not provide any significant shielding from erosion even though lines of force are made near-parallel to that section of the wall. The shape of the channel alone also does not determine the effectiveness of magnetic shielding. For example, Figure 8-middle depicts a configuration with a diverging channel section but because most of the lines that intersect it are associated with low potential and high electron temperature this arrangement too would not achieve strong shielding.

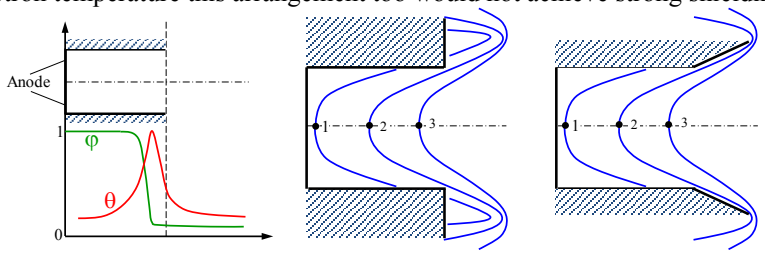

Figure 7. Left: Typical profile of the non-dimensional plasma potential $\varphi \equiv \phi/\phi_{max}$ and electron temperature $\theta \equiv T_e/T_{e,max}$ along the acceleration channel centerline. Middle and right: Configurations with strong magnetic shielding of the (shaded) walls near the channel exit. The three numbered locations at the centerline correspond to $\varphi_1 \approx \varphi_2 \approx 1$, $\theta_1, \theta_2 << 1$ and $\varphi_3 << 1$, $\theta_3 \approx 1$. The magnetic field topologies, shown here for illustration only, are freehand drawings and do not match topologies in any specific thruster discussed herein.

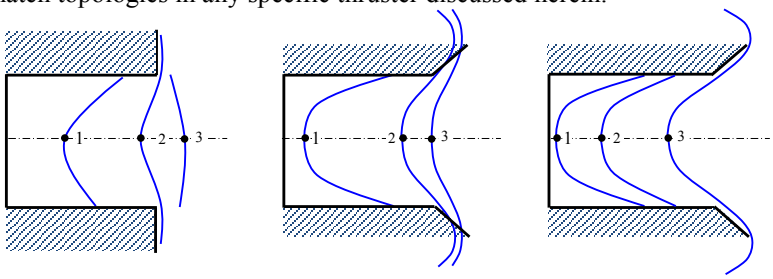

Figure 8. Configurations with weak or no magnetic shielding of the (shaded) walls near the channel exit. Referring to the generic profiles for φ and θ in Figure 7-left, the three numbered locations at the centerline correspond to the following. Left and middle: $\varphi_1 \approx 1$, $\theta_1 << 1$, $\varphi_2 << 1$, $\theta_2 \approx 1$, $\varphi_3 << 1$, $\theta_3 \lesssim 1$. Right: $\varphi_1 \approx \varphi_2 \approx 1$, $\theta_1, \theta_2 << 1$ and $\varphi_3 << 1$, $\theta_3 \approx 1$. The magnetic field topologies, shown here for illustration only, are freehand drawings and do not match topologies in any specific thruster discussed herein.

These principles have been employed to modify the magnetic field and channel geometry of the H6 thruster with the goal of demonstrating magnetic shielding in the laboratory at a single operating point. Hall2De has been used to guide the design. The design iteration cycle began with a preliminary phase in which the field topology near the channel walls was modified until magnetic shielding of the walls was achieved, by superimposing to the existing magnetic field the (idealized) solution of current-carrying coils. This preliminary solution guided the design of the magnetic circuit, which was carried out using MagNet (v7). MagNet is a 2-D/3-D electromagnetic field simulation software developed by Infolytica Corporation[29] that has been used for many years at various institutions of government, industry and academia to design magnetic circuits for Hall thrusters. The design cycle may require one or more iterations to achieve effective magnetic shielding, high propulsive performance and high magnetic circuit efficiency.

Figure 9 depicts profiles of the solution along the channel centerline obtained by numerical simulation of the MS configuration. Computed values related to thruster performance are listed in Table 1. By contrast to our previous simulations with the BPT-40009 for which plasma and performance measurements existed in both the unshielded and shielded geometries, no data exist for the H6 MS design. Hence our approach regarding the non-classical collision frequency ν_α was to assume that similar non-classical physics persist in the two configurations and impose the same functional form of ν_α in the two configurations. The non-classical electron collision frequencies and Hall parameter are compared in Figure 9-right. To attain the operating discharge current (20 A) in the MS configuration, ν_α was altered marginally from that used in the BL but no additional effort was undertaken to improve the correlation between measured and computed thrust (Table 1) by altering further the ν_α profile. As it will be argued below such improvements are in fact not critical in this first phase of the design.

The electron temperature and plasma potential in Figure 9-left exhibit trends that are qualitatively similar to those in the BL configuration. One difference is that the near-exit axial electric field along the channel centerline is found to be smaller in the MS configuration compared to that in the BL, which contributes to the lower thrust that has been computed in the MS configuration (Table 1). This lower value however does not imply that performance will in fact also be lower when the MS thruster is tested because the plasma potential in this region depends, in part, on ν_α the precise form of which is presently unknown. Moreover, it is noted that when the BPT-4000 was tested at JPL performance in the unshielded and shielded configurations was found to be effectively the same.[30] It is possible that the non-classical transport physics are different in the two H6 configurations, inducing different behavior of ν_α; indeed this was one of our findings in the BPT-4000 simulations.9 But since the erosion rates in the MS configuration are at least a few orders of magnitude less than those in the BL, a result that is quantified further in Sec. II-E, differences of several percent points in the computed thrust and a few factors in the plasma potential near the channel exit are of little consequence on erosion. This is because the plasma in the shielded regions near the channel walls is, *by design*, sustained at values of the potential that are as close as possible to the discharge voltage (see also Figure 10-top-right). As explained previously this is accomplished with magnetic field lines that extend deep into the channel where the electric field is negligible and largely independent of the near-exit plasma.

Similar arguments may be made regarding the electron temperature. Its maximum value is found to be approximately 10 eV higher in the MS design (compare Figure 6-left with Figure 9-left). Similar discrepancy in the two configurations is observed near the channel exit. While it may be argued that elevated electron temperatures can be expected in MS configurations due to reductions of power deposition to the walls,[31] at present, the elusive nature of the electron transport physics and the uncertainty on the true wall emission/absorption characteristics in these devices (e.g. see Refs.32, 33) do not yet permit the prediction of the precise electron temperature near the channel exit. However, as in the case of the plasma potential, it is argued that such precision is of little consequence on erosion because to reduce the sheath energy of ions, electrons near the shielded channel walls are, *by design*, cold. This is achieved by taking advantage of the isothermal properties of magnetic field and exploiting those lines that extend deep into the channel where it is known that electrons are indeed much colder (see for example Figure 10-middle). The cold-electron regions near the shielded channel walls are therefore not affected significantly by the hotter-electron regions near the channel exit. That is to say, the lines here serve as an effective thermal insulation for the cold electrons near the surface. Consequently, so long as the computed electron temperature is comparable to the (well-known by now) qualitative profile depicted in Figures 6 and 9 the precise maximum value of the electron temperature and its location relative to the channel exit is of little consequence on magnetic shielding. While the design of MS thrusters may indeed proceed with experimentally guided forms of ν_α for the abovementioned reasons, it should be recognized that until the true electron transport physics in Hall thrusters have been identified the risk and number of design iterations between numerical simulation and experiment will remain higher than desired. As part of our ongoing investigations we plan to revisit ν_α and related physics in the phase II of the thruster design.

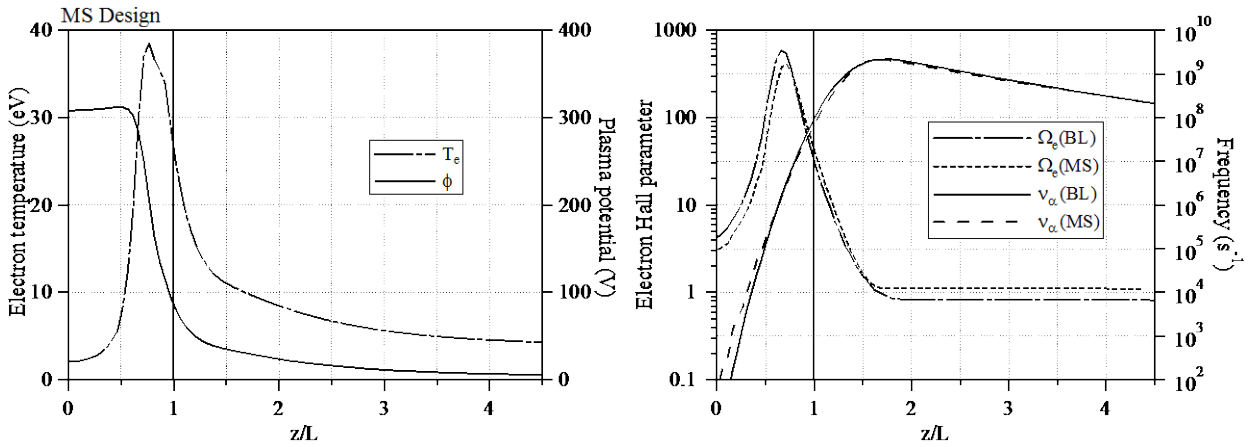

Figure 9. Axial profiles along the channel centerline in the MS configuration of the H6 Hall thruster. Left: Numerical simulation results for the electron temperature and plasma potential. (Plasma diagnostics are planned in phase II of the design effort). Right: Comparison of the electron Hall parameter and collision frequency ν_α between the BL and MS configurations.

Selected contoured plots for the BL and MS configurations are compared in Figure 10. For reference, the locations of the magnet corners in both configurations are also shown. Results that are pertinent to channel erosion are plotted in Figure 11. The effect of the thermalized equipotentialization of the lines of force can be seen in Figure 10-top. We compute a reduction in the plasma potential of only 6-13 V along the MS outer and inner diverging wall sections compared to a significant drop of >270 V near the channel exit of the BL configuration. More detailed results along the walls are provided in Figure 11-top-left. Thus, acceleration of ions near the BL walls is considerably higher compared to that near the MS walls. This higher acceleration, in turn, increases the kinetic energy with which ions enter the sheath. Figure 11-top-right shows that the largest reduction of kinetic energy in the MS configuration is about one order of magnitude and occurs at $0.8<z/L<0.9$. Upstream of $z/L\sim0.9$ the difference decreases and the energy in the two configurations becomes comparable. The energy in the MS configuration increases here, despite little change of the plasma potential adjacent to the channel surfaces (see Figure 11-top-left), because the high concentration of magnetic field lines near the corner at the downstream end of the channel increases the component of the electric field in the direction parallel to the surface. The convergence of the plasma potential contours near the channel corner can be seen clearly in Figure 10-top-right. As it will be discussed later however this increase of the ion kinetic energy occurs in a region where the ion number density has decreased significantly. Thus, there is insufficient flux to cause any detectable erosion.

The same principle that leads to the thermalized equipotentialization of the lines of force is responsible also for their isothermalization. Thus, since magnetic field lines are nearly isothermal in the acceleration channel, those lines that graze the corner formed by the cylindrical and diverging sections of the channel wall in the MS configuration are associated also with low values of the electron temperature because they extend deep into the acceleration channel. There the electrons are considerably colder as shown for example in Figure 10-middle. The comparison of the two configurations (Figure 10-middle and Figure 11-middle-left) shows a significant reduction of the temperature in these highly shielded regions. Because the electron temperature is reduced a decline of the sheath fall along these surfaces is also induced. Figure 11-middle-right shows a reduction of the sheath energy of about one order of magnitude in the last ~25% of the channel.

A third effect is induced, by design, in the diverging channel section and is related to the spatial distribution of the plasma potential. In particular, because near the MS diverging walls the component of the electric field parallel to them is reduced significantly, the acceleration of ions is mostly perpendicular and away from the walls. Moreover, this acceleration becomes significant largely because the electric field in this region also is significant; note in Figure 10-top-right that the plasma potential falls by about the full discharge voltage within less than half the length of the diverging segment of the channel, in a direction perpendicular to it. Acceleration of ions in this manner leads to much lower number of charged particles in these highly shielded regions of the channel. Referring to Figure 11-bottom-left the Xe^+ number density near the channel corners is found to be more than a few orders of magnitude less in the MS configuration than in the BL. The significance of this on erosion is that the total ion flux to the wall is reduced significantly as well. Figure 10-bottom compares contours of the electron number density overlaid by the flux vector field of Xe^+. Figure 11-bottom-right plots the incident current density of Xe^+ along the channel walls.

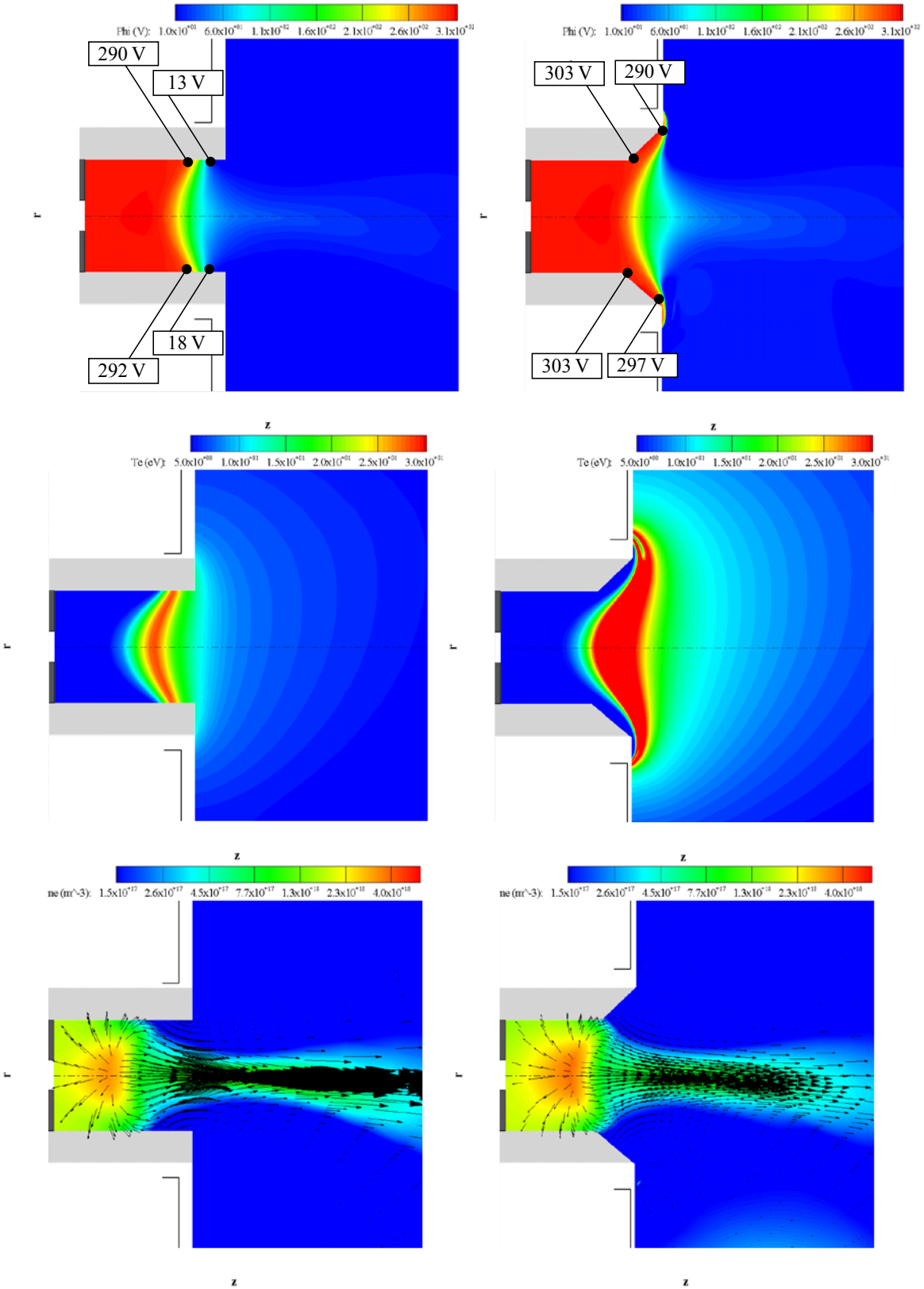

Figure 10. Comparison of the numerical simulation results in the BL (left) and MS (right) thruster configurations. Top: Plasma potential. Middle: Electron temperature. Bottom: Electron number density overlaid by trajectories of singly-charged ion current density.

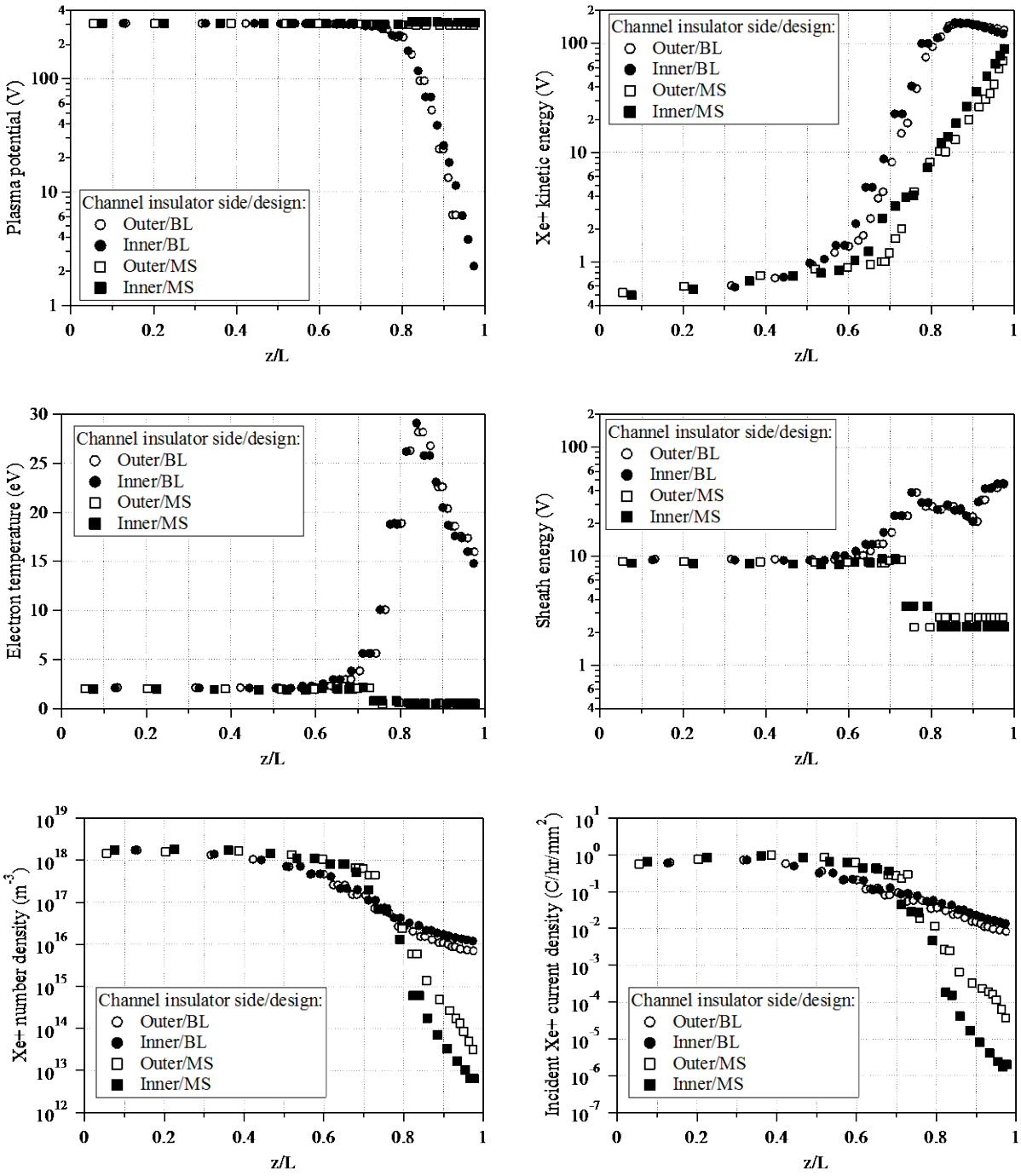

Figure 11. Hall2De results pertinent to erosion along the outer and inner channel insulators of the H6 Hall thruster. Chamfering of the channel in the MS configuration begins at approximately z/L=0.72. Top: Plasma potential (left) and impact kinetic energy of singly-charged xenon ions (Xe^+). Middle: Electron temperature (left) and sheath energy (right). Bottom: Number density (left) and current density (right) of incident Xe^+. Notes: (1) the sought-after profiles of high plasma potential and low electron temperature in the MS configuration are illustrated clearly in the top-left and middle-left plots, (2) reductions of the ion kinetic and sheath energies that exceed cumulatively one order of magnitude are achieved in regions of the thruster channel that typically exhibit the highest erosion rates, (3) the high electric field established by the shielding topology of the magnetic field is directed largely perpendicular to the channel wall, accelerating ions away from the surfaces, which reduces the incident ion flux by >3 orders of magnitude near the channel exit (bottom-right).

E. **Channel erosion**

In this section we quantify the erosion rates in the two configurations. In phase II of the design we plan to perform direct measurements of the flux and ion energy to the channel surfaces and compare erosion results with the theoretical predictions. The diagnostics and test plan are described in Sec. III. The sputtering erosion rate (ε) due to ion bombardment is given by,

$$\varepsilon = j_{i\perp} Y \tag{II-1}$$

where the incident ion current density perpendicular to the channel wall $j_{i\perp}$ is dependent on the ion number density (n_i) and the ion velocity (u_i) at the wall. The sputtering yield (Y) of the channel material is a function of the ion impact energy (K) and incidence angle (θ). Because ions must traverse a sheath before striking the wall, the total impact energy is the sum of the kinetic energy $K_i=\frac{1}{2}m_i u_i^2$ ions of mass m_i have acquired in the plasma upon entrance to the sheath, and the sheath potential energy denoted as $\Delta\phi$. That is,

$$j_{i\perp} = j_{i\perp}\left(q_i, n_i, u_{i\perp}\right) \qquad Y = Y\left(K_i + \Delta\phi, \theta\right) \tag{II-2}$$

where q_i is the ion charge. The potential energy $\Delta\phi$ is determined based on the solution to the one-dimensional sheath equations in the presence of secondary electron emission provided by Hobbs and Wesson.[22] In the numerical simulations we use the vertex-centered ion velocities and the element-centered ion density at each computational element adjacent to the wall boundary to determine the total impact energy $K=K_i+\Delta\phi$ and angle θ. Then the sputtering yield is determined using the fitting functions $f_K(K_i+\Delta\phi)$[34] for the energy dependence at zero angle of incidence, and $f_\theta(\theta)$[35] for the angle dependence as follows:

$$Y = f_\theta(\theta) f_K(K). \tag{II-3}$$

The fitting functions f_K and f_θ are plotted in Figure 12.

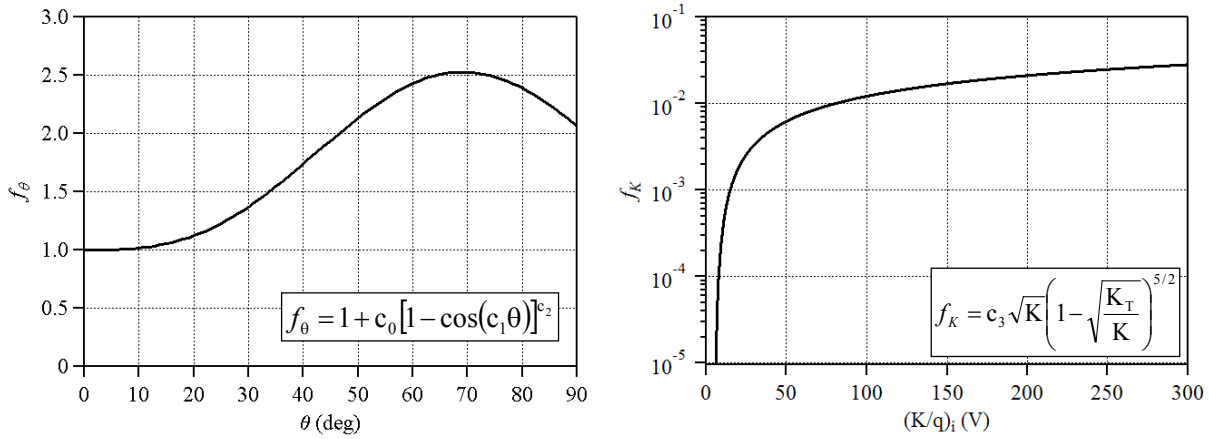

Figure 12. Fitting functions for the sputtering yield of the H6 channel material (see Eq. (II-3)**)**. The coefficients are c_0=0.52663, c_1=2.60506, c_2=1.53462, c_3=0.0023 and K_T=5.1.

The erosion rates along the outer and inner channel insulators from the Hall2De simulations are plotted in Figure 13. In the last ~30% of the channel the simulations predict that the erosion rates in the MS design are approximately 10^{-5} – 10^{-7} mm/h, a range that is 2-4 orders of magnitude lower than that in the BL channel. As pointed out by Mikellides *et al*.9 the higher rates (~10^{-5} mm/h) can be improved significantly by cambering the corner formed by the cylindrical and diverging sections of the channel to follow the local curvature of the magnetic field lines. Improvements of this kind are planned in more advanced designs of MS Hall thrusters.

For the majority of the channel it is found that the two configurations exhibit similar erosion rates, as expected. For $z/L \lesssim 0.6$ erosion rates in both configurations are in the order of $1\text{-}3\times10^{-4}$ mm/h. Such values are high enough to suggest that erosion of the order of ~1 mm may be detected over several thousand hours. However, as shown in Figure 11-top-right and -middle-right, along these portions of the channel the total ion impact energy has fallen below ~10 V where there exists significant uncertainty about the true sputtering yield. For the material used in

the H6 channel insulators there are only limited measurements of the sputtering yield, most of which provide values only for energies that exceeded 100 V. The most recent data for energies <100 V were produced by Rubin *et al*.[36] Based on a comparison of the fitting function f_K (Figure 12-right) with Rubin's data, Shastry[37] showed that the measured yield values were higher by factors ranging 2-5 for energies >100 V. With a new set of fitting functions based on Rubin's data, Shastry suggested that the sputtering yield exhibits a steeper fall at low energies, dropping below 10^{-4} between 30-45 V instead of the ~10 V predicted by f_K. However, Rubin *et al*. acknowledge that their values are higher than published data and no explanations were provided for this discrepancy. Therefore, the sputtering yield in this range of ion energies (<50 V) remains highly uncertain. For consistency with our computed erosion rates in the BPT-40009 the results for the H6 in Figure 13 are presented for the same sputtering yield fitting functions (as given in Figure 12 and in Ref. 9). However, to illustrate the impact of the uncertainty in the sputtering yield on the erosion predictions of Figure 13 we performed a sensitivity calculation the results of which are shown in Figure 14. While retaining similar values of f_K at energies >100 V, we compute that for only a ~5-V increase in the value of K_T a reduction of 4-5 orders of magnitude occurs in the erosion rate. Thus, erosion rates for z/L$\lesssim$ 0.7 in both configurations could be significantly lower than the computed values due to the low ion impact energies ($\lesssim$ 30 V) in these regions. For the same reason, the erosion rate in the MS configuration along the highly shielded regions could also be significantly lower than the computed values.

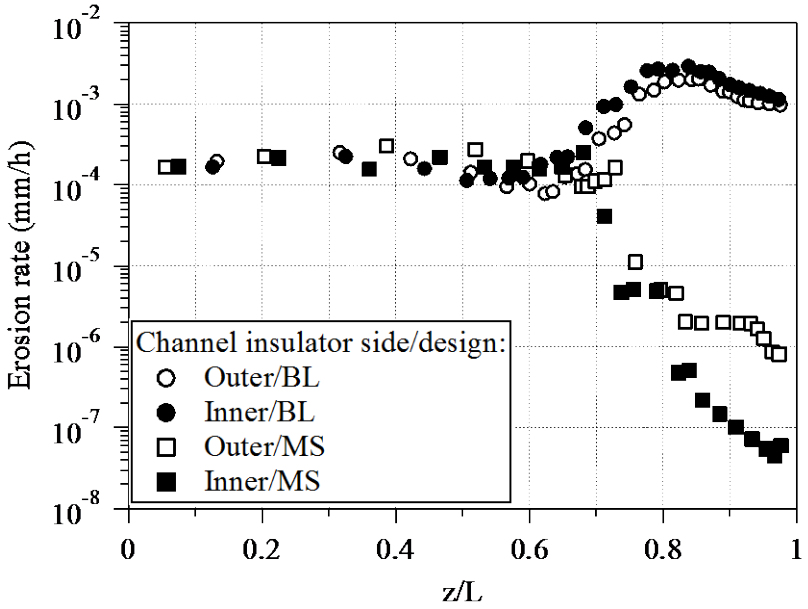

Figure 13. Erosion rate along the outer and inner channel insulators of the H6 Hall thruster. The rates have been determined by numerical simulation of the BL and MS configurations. The erosion rates in the MS configuration are designed to be 2-4 orders of magnitude lower than those in the BL configuration along regions of the channel where most wear would occur (z/L>0.7).

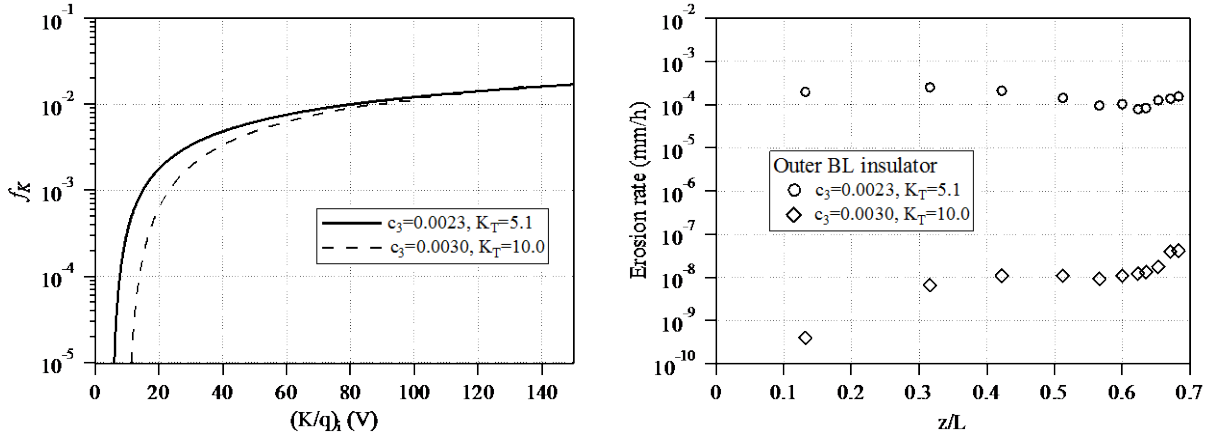

Figure 14. Sensitivity of computed erosion rates on the sputtering yield fitting function f_K at low ion impact energies.

III. Experiment Plan for the Demonstration of Magnetic Shielding in the Laboratory

A series of experiments are now being conducted to demonstrate magnetic shielding in the modified (MS) configuration of the H6 laboratory Hall thruster. These experiments are part of a larger systematic effort to explore the implications of magnetic shielding on lifetime that will ultimately extend these studies to large throttling ranges and advanced thruster designs. The present experiments will compare the operating and thermal characteristics, plasma properties, and erosion rates of the discharge chamber resulting from the BL and MS configurations described previously. At the time of this writing, the first series of these experiments has just begun. In this section, we describe the test plan for the experimental campaign. Future publications will present the results of the experiments described below.

The primary objectives of the test campaign are as follows:

(1) Demonstrate that an existing Hall thruster utilizing a plasma-lens magnetic field4 may be modified to enable magnetic shielding thereby realizing effective lifetimes much greater than previous capabilities.
(2) Demonstrate that magnetic shielding can be applied to Hall thrusters that are of significantly different design than the BPT-4000.
(3) Validate the physics-based design methodology for implementing magnetic shielding in an existing thruster for a single operating point.
(4) Quantify the impact of any performance differences between the two thruster configurations.
(5) Quantify the effects of magnetic shielding on the discharge chamber thermal characteristics.
(6) Measure the plasma properties of a MS thruster to a much higher level of detail than was possible during qualification testing of the BPT-4000.7

A. Experimental Apparatus

1. H6 Hall Thruster

The H6 is a nominally 6 kW laboratory Hall thruster that was developed as a testbed for studies of thruster physics and developments in diagnostics and thruster technology.[38] The thruster was a joint development between AFRL, JPL and the University of Michigan, and continues to be studied at those institutes. The thruster is capable of throttling over 0.6-12 kW discharge power, 1000-3000 s specific impulse, and 50-500 mN thrust. Performance at 6 kW discharge power recently measured at JPL is shown in Figure 15. Over 70% total efficiency is achieved at discharge voltage of 800 V. At the nominal 300 V, 6-kW condition, thrust, total specific impulse, and total efficiency are 406 mN[§], 1970 s, and 65%, respectively.

For these experiments, changes to the thruster are being made to the magnetic circuit and discharge chamber. New pole pieces have been fabricated for the magnetic circuit that will be exchanged with existing parts. The changes are confined to the inner and outer front pole pieces and the inner and outer screens. No changes are being made to the electromagnets or back pole piece. The discharge chamber of the existing thruster is designed with replaceable boron nitride inserts. These inserts have axial lengths that overlap the erosion zone (see Figure 13), such that new inserts can be fabricated to accommodate design changes or wall diagnostics.[37,39] New inserts have been fabricated for these experiments with geometries that are compatible with magnetic shielding of the walls.

2. Vacuum Facility

The experiments are being performed in the 3 m diameter by 10 m long Endurance Test Facility (ETF) at JPL. The facility is cryogenically pumped and is lined with graphite panels to minimize back-sputtered material to thruster surfaces. Base pressures between 10^{-8} and 10^{-7} torr are routinely achieved. The pumping speed of the facility is approximately 200,000 l/s.

3. Diagnostics

Multiple diagnostics will be deployed to measure the changes induced in the two thruster configurations. The diagnostics are similar to those described in Ref. 30. The specific diagnostics will include:

(1) Thrust stand for measuring thruster performance (thrust, specific impulse, efficiency).
(2) Discharge current probes for measuring anode current oscillations.
(3) Far-field plume probes for measuring ion flux, plasma potential, species fractions, and ion energy.

[§] This value is different than that in Table 1 because a trim coil was used in the magnetic circuit that produced the higher thrust value.

(4) Near-field plume probes for measuring ion flux, plasma potential, electron temperature, and plasma density.
(5) Reciprocating probes injected axially in to the discharge chamber to measure plasma potential and electron temperature.
(6) Flush-mounted wall probes for measuring plasma potential, electron temperature, ion current density, and ion incidence angle. The approach will follow the techniques developed by Shastry in Refs. 37 and 39.
(7) Erosion diagnostics for quantifying erosion rates. Laser profilometry and surface layer activation techniques will be used. Data from the flush-mounted wall probes will also be used to calculate erosion rates (Refs. 37 and 39).
(8) Thermocouples and a thermal camera for measuring the thruster temperature distribution.
(9) Residual gas analyzer (RGA) for measuring the background gases present in the facility and a quartz crystal microbalance (QCM) mounted near the thruster for measuring the back-sputter rate of carbon.
(10) 3-axis gaussmeter for measuring the applied magnetic field.

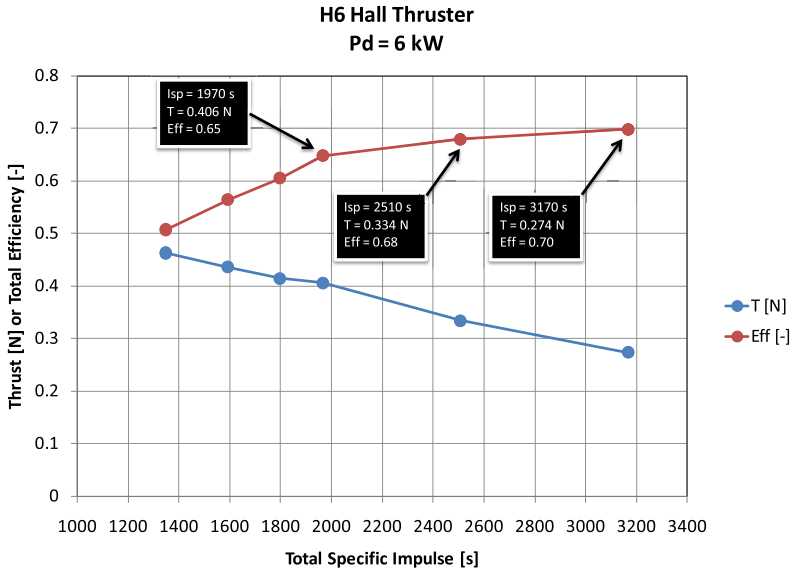

Figure 15. Left: Performance of the H6 Hall thruster at constant discharge power of 6 kW. Over 70% total efficiency is achieved at discharge voltage of 800 V. At the nominal 300 V, 6 kW condition, thrust, total specific impulse, and total efficiency are 406 mN[§], 1970 s, and 65%, respectively.

B. Test sequence

The two thruster configurations will be tested at JPL in phase II of the effort and each of the diagnostics described above will be used. Both configurations of the thruster will be operated at 300 V, 20 A. The sequence of the experiments will be as follows:

BL thruster configuration
(1) Pre-test discharge chamber profilometry measurements.
(2) Magnetic field measurements.
(3) Performance, plasma, and erosion measurements at 300 V, 20 A.
(4) Post-test discharge chamber profilometry measurements.

MS thruster configuration
(1) Modification of the magnetic circuit and discharge chamber to enable magnetic shielding.
(2) Pre-test discharge chamber profilometry measurements.
(3) Magnetic field measurements.
(4) Performance, plasma, and erosion measurements at 300 V, 20 A.
(5) Post-test discharge chamber profilometry measurements.

IV. Conclusion

Numerical simulations suggested recently that Hall thrusters can be designed to have MS acceleration channels, a technique that could reduce channel erosion by several orders of magnitude. The elimination of erosion in these thrusters would retire the risk associated with their throughput capability and enable a wide range of deep-space missions for NASA. In 2009 a proof-of-principle effort began at JPL with two major objectives: (1) to demonstrate understanding of magnetic shielding physics and (2) to demonstrate capacity to design Hall thrusters with extremely long life based on this technique. The effort consisted of two main phases. The first involved the modification of the acceleration channel and magnetic circuit in an existing 6-kW laboratory Hall thruster. The modifications were guided by extensive numerical simulation. The new MS thruster configuration has been designed to (1) reduce the kinetic and sheath energy of incident ions by >1 order of magnitude and, (2) reduce the incident ion flux by >3 orders of magnitude. The erosion rates in the MS configuration are predicted to be 2-4 orders of magnitude lower than the highest erosion rates found in the BL configuration. In the (ongoing) second and final phase of the effort direct measurements of the ion flux and energy will be conducted along the channel walls in both thruster configurations to establish the feasibility of magnetic shielding in Hall thrusters.

Acknowledgments

The research described in this paper was carried out by the Jet Propulsion Laboratory, California Institute of Technology, under a contract with the National Aeronautics and Space Administration. Reference herein to any specific commercial product, process, or service by trade name, trademark, manufacturer, or otherwise, does not constitute or imply its endorsement by the United States Government or the Jet Propulsion Laboratory, California Institute of Technology.

References

[1] A. I. Morozov, and V. V. Savelyev, "Fundamentals of Stationary Plasma Thruster Theory," *Reviews of Plasma Physics*, 21, 203 (2000).
[2] D. Manzella, R. Jankovsky, and R. R. Hofer, "Laboratory Model 50 kW Hall Thruster," AIAA Paper No. 02-3676 (2002).
[3] P. Peterson, D. Manzella, and J. John, "The Performance and Wear Characterization of a High-Power High-Isp NASA Hall Thruster," AIAA Paper No. 05-4243 (2005).
[4] R. R. Hofer, and A. D. Gallimore, "High-Specific Impulse Hall Thrusters, Part 1: Influence of Current Density and Magnetic Field," *J. Propul. Power*, 22, 4, 721-731 (2006).
[5] B. Welander, *et al*., "Life and Operating Range Extension of the BPT-4000 Qualification Model Hall Thruster," AIAA Paper No. 06-5263 (2006).
[6] H. Kamhawi, D. H. Manzella, L. Pinero, T. Haag, A. Mathers, and H. Liles, "In-Space Propulsion High Voltage Hall Accelerator Development Project Overview," AIAA Paper No. 10-6860 (2010).
[7] K. H. De Grys, A. Mathers, B. Welander, and V. Khayms, "Demonstration of 10,400 Hours of Operation on 4.5 kW Qualification Model Hall Thruster," AIAA Paper No. 10-6698 (2010).
[8] I. G. Mikellides, I. Katz, R. R. Hofer, and D. M. Goebel, "Hall-Effect Thruster Simulations with 2-D Electron Transport and Hydrodynamic Ions," IEPC Paper No. 09-114 (2009).
[9] I. G. Mikellides, I. Katz, R. R. Hofer, D. M. Goebel, K. de Grys, and A. Mathers, "Magnetic Shielding of the Channel Walls in a Hall Plasma Accelerator," *Phys. Plasmas*, 18, 3, 033501 1-18 (2011).
[10] G. Kornfeld, N. Koch, H. Harmann, "Physics and Evolution of HEMP-Thrusters," IEPC Paper No. 07-108 (2007).
[11] D. G. Courtney, P. Lozanoy, and M. Martinez-Sanchez, "Continued Investigation of Diverging Cusped Field Thruster," AIAA Paper No. 08-4631 (2008).
[12] I. G. Mikellides, I. Katz, D. M. Goebel, K. K. Jameson, and J. E. Polk, "Wear Mechanisms in Electron Sources for Ion Propulsion, II: Discharge Hollow Cathode," *J. Propul. Power*, 24, 866-879 (2008).
[13] I. G. Mikellides, and I. Katz, "Wear Mechanisms in Electron Sources for Ion Propulsion, I: Neutralizer Hollow Cathode," *J. Propul. Power*, 24, 855-865 (2008).
[14] J. M. Fife, "Hybrid-PIC Modeling and Electrostatic Probe Survey of Hall Thrusters," Ph.D. thesis, Massachusetts Institute of Technology, 1998.
[15] F. I. Parra, E. Ahedo, J. M. Fife, and M. Martinez-Sanchez, "A Two-Dimensional Hybrid Model of the Hall Thruster Discharge," *J. Appl. Phys.*, 100, 023304 (2006).

[16] A. Ducrocq, J. C. Adam, A. Héron, and G. Laval, "High-Frequency Electron Drift Instability in the Cross-Field Configuration of Hall Thrusters," *Phys. Plasmas,* 13, 102111 (2006).
[17] A. Lazurenko, T. Dudok de Wit, C. Cavoit, V. Krasnoselskikh, A. Bouchoule, and M. Dudeck, "Determination of the Electron Anomalous Mobility Through Measurements of Turbulent Magnetic Field In Hall Thrusters," *Phys. Plasmas*, 14, 033504 (2007).
[18] C. Boniface, L. Garrigues, G. J. M. Hagelaar, J. P. Boeuf, D. Gawron, and S. Mazouffre, "Anomalous Cross Field Electron Transport in a Hall Effect Thruster," *Appl. Phys. Lett*., 89, 161503 (2006).
[19] D. Bohm, E. Burhop, and H. Massey, *Characteristics of Electrical Discharges in Magnetic Fields* (McGraw-Hill, New York, 1949), p. 77.
[20] S. I. Braginskii, "Transport Properties in a Plasma," *Reviews of Plasma Physics*, (Consultants Bureau, New York, 1965), Vol. 1, p. 205.
[21] I. G. Mikellides, I. Katz, R. R. Hofer, D. M. Goebel, K. H. de Grys, and A. Mathers, "Magnetic Shielding of the Acceleration Channel Walls in a Long-Life Hall Thruster," AIAA Paper No. 10-6942 (2010).
[22] G. D. Hobbs, and J. A. Wesson, "Heat Flow Through a Langmuir Sheath in the Presence of Electron Emission," *Plasma Phys.*, 9, 85 (1967).
[23] I. Katz, and I. G. Mikellides, "Neutral Gas Free Molecular Flow Algorithm Including Ionization and Walls for Use in Plasma Simulations," *J. Comput. Phys*., 230, 4, 1454-1464 (2011).
[24] B. M. Reid, "The Influence of Neutral Flow Rate in the Operation of Hall Thrusters," Ph.D. Thesis, Aerospace Engineering, University of Michigan, 2009.
[25] K. K. Jameson, "Investigation of Hollow Cathode Effects on Total Thruster Efficiency in a 6 kW Hall Thruster," Ph.D. Dissertation, Aerospace Engineering, University of California, Los Angeles, 2008.
[26] R. R. Hofer, *et al.*, "Efficacy of Electron Mobility Models in Hybrid-PIC Hall Thruster Simulations," AIAA Paper No. 08-4924 (2008).
[27] G. Hagelaar, J. Bareilles, L. Garrigues, and J. P. Boeuf, "Two-Dimensional Model of a Stationary Plasma Thruster," *J. Appl. Phys.,* 91, 5592 (2002).
[28] J. Bareilles, G. Hagelaar, L. Garrigues, C. Boniface, and J. Boeufa, "Critical Assessment of a Two-Dimensional Hybrid Hall Thruster Model: Comparisons with Experiments," *Phys. Plasmas*, 11, 6 (2004).
[29] http://www.infolytica.com/en/products/magnet/
[30] R. R. Hofer, D. M. Goebel, J. S. Snyder, and I. Sandler, "BPT-4000 Hall Thruster Extended Power Throttling Range Characterization for NASA Science Missions," IEPC Paper No. 09-085 (2009).
[31] I. Katz and I. G. Mikellides, "Channel Wall Plasma Thermal Loads in Hall Effect Thrusters with Magnetic Shielding," 47th AIAA/ASME/SAE/ASEE Joint Propulsion Conference & Exhibit, AIAA, Reston, VA (submitted for publication).
[32] Y. Raitses, D. Staack, M. Keidar, and N. J. Fisch, "Electron-wall Interaction in Hall Thrusters," *Phys. Plasmas*, 12, 057104 (2005).
[33] E. Ahedo, and F. I. Parra, "Partial Trapping of Secondary-Electron Emission in a Hall Thruster Plasma," *Phys. Plasmas* 12, 073503 (2005).
[34] Y. Yamamura, and H. Tawara, "Energy Dependence of Ion-Induced Sputtering Yields from Monatomic Solids at Normal Incidence," *Atomic Data and Nuclear Data Tables*, 62, 149-253 (1996).
[35] E. J., Pencil, T., Randolph, and D. H. Manzella, "End-of-Life Stationary Plasma Thruster Far-Field Plume Characterization," AIAA Paper No. 96-2709 (1996).
[36] B. Rubin, J. L. Topper, and A. P. Yalin, "Total and Differential Sputter Yields of Boron Nitride Measured by Quartz Crystal Microbalance," *J. Phys. D: Appl. Phys.*, 42, 205205 1-11 (2009).
[37] R. Shastry, "Experimental Characterization of the Near-Wall Region in Hall Thrusters and Its Implications on Performance and Lifetime," Ph.D. Dissertation, Aerospace Engineering, University of Michigan, 2011.
[38] J. M. Haas, R. R. Hofer, D. L. Brown, B. M. Reid, and A. D. Gallimore, "Design of the H6 Hall Thruster for High Thrust/Power Investigation," 54th JANNAF Propulsion Meeting, Denver, CO, May 14-17, 2007.
[39] R. Shastry, A. D. Gallimore, and R. R. Hofer, "Experimental Characterization of the Near-Wall Plasma in a 6-kW Hall Thruster and Comparison to Simulation," 47th AIAA/ASME/SAE/ASEE Joint Propulsion Conference & Exhibit, AIAA, Reston, VA (submitted for publication).